Nano Research 2016, 9(2): 442–450
DOI 10.1007/s12274-015-0925-5
Research Article
ISSN 1998-0124
CN 11-5974/O4

Multifunctional silver film with superhydrophobic and antibacterial properties

Ping Che[1], Wei Liu[1,2], Xiaoxue Chang[3], Anhe Wang[4], and Yongsheng Han[2] (✉)

[1] *School of Chemistry and Biological Engineering, University of Science & Technology Beijing, Beijing 100083, China*
[2] *State Key Laboratory of Multiphase Complex Systems, Institute of Process Engineering, Chinese Academy of Sciences, Beijing 100190, China*
[3] *State Key Laboratory of Theoretical Physics, Institute of Theoretical Physics, Chinese Academy of Science, Beijing 100190, China*
[4] *Key Laboratory of Colloid and Interface Sciences, Institute of Chemistry, Chinese Academy of Sciences, Beijing 100190, China*

Received: 24 July 2015
Revised: 18 September 2015
Accepted: 15 October 2015

KEYWORDS
hydrophobicity,
antibacterial,
silver film,
electrodeposition

ABSTRACT

Material properties are strongly dependent on material structure. The large diversity and complexity of material structures provide significant opportunities to improve the properties of the materials, expanding their applications. Here, we discuss the fabrication of a multifunctional silver film prepared by controlling the nucleation and growth of silver particles. Silver films with high hydrophobicity and antibacterial activity were fabricated by adopting an electrochemical approach. The dependence of the hydrophobic and antibacterial properties on the size and shape of the silver particles was first investigated. Small-sized silver particles exhibited a high antibacterial rate, while a porous silver film composed of dendritic particles showed a significant hydrophobic activity. By regulating the reaction time, current density, and silver salt concentration, a silver film with a contact angle of 150.9° and an antibacterial rate of 54.7% was synthesized. This study demonstrates that finding a compromise between different material structures is a suitable way to fabricate multifunctional devices.

1 Introduction

In nature, leaves are not only biosystems for the production of oxygen via photosynthesis, but also interfaces that promote breath and evaporation [1–3]. Some leaves even possess a rough surface, exhibiting excellent water collection properties [4]. Inspired by nature, scientists have developed a great interest in fabricating multifunctional materials with different capacities [5, 6]. For example, hydrophobicity and antibacterial protection are two critical requirements for a sea vessel. A high hydrophobicity improves the ship speed, while an effective antibacterial protection results in a considerably longer ship life. In the past, copper was used as a warship coating material to obtain protection against microorganisms and increase the ship flexibility in battle [7, 8]. Modern fishermen simply coat their ships with pesticides before launching; if the

Address correspondence to yshan@ipe.ac.cn

environmental issues are ignored, pesticides provide a good protection against microorganisms [9, 10]. In this work, we investigate the possibility to obtain a hydrophobic and antibacterially protected ship surface, providing at the same time the additional benefits of environmentally friendliness and cost effectiveness.

Silver is well known for its antibacterial activity [11–13]. Diverse silver species in the form of ions, particles, and salts, have been investigated for antibiotic reactions, showing different cell killing mechanisms. For example, silver ions are believed to adsorb on the negatively charged bacterial cell wall, deactivating cellular enzymes, disrupting membrane permeability, and ultimately leading to cell lysis and death [14]. Silver particles, especially silver nanoparticles, kill bacteria by generating reactive oxygen species (ROS), which break the cell membrane and proteins [14–16]. Besides, silver nanoparticles are also able to penetrate inside the bacteria and cause further damage [17]. A plausible mechanism of silver toxicity has been proposed, and involves the disruption of the mitochondrial respiratory chain by the silver nanoparticles; this leads to the production of ROS and interruption of ATP synthesis, causing, in turn, DNA damage [18]. Therefore, the size of the silver particles is critical for their antibacterial activity, as it not only influences the production of silver ions and ROS, but it also determines the particle distribution around the cells [19–24]. Furthermore, nanoprisms and, at a lower extent, nanorods present higher antibacterial activity than nanospheres [25, 26] owing to the large exposure of high-atomic-density {111} facets [27–30]. In addition to the antibacterial activity, the hydrophobicity of silver structures has been well documented. For example, via galvanic deposition of silver films on a metal substrate, Xu et al. reported a facile way to generate a superhydrophobic surface subsequently passivated by n-octadecanethiol self-assembled monolayers [31]. Superhydrophobic surfaces [32–35] usually have a complex structure with remarkable roughness [36], which is attributed to the improvement of our understanding of the mechanism of superhydrophobicity. As superhydrophobicity and antibacterial activity are properties typically exhibited by different types of silver structures, finding a structural compromise to obtain a silver product exhibiting both properties is a difficult challenge.

In this work, we tried to tackle this challenge. Electrodeposition was employed to fabricate a silver film on the surface of a metal substrate. Different silver film morphologies were produced and tested for hydrophobicity and antibacterial activity. After a detailed investigation on the dependence of these two properties on the silver morphology, the optimal morphology was determined, and a multifunctional silver film showing both properties was realized.

2 Experimental

2.1 Materials

Silver nitrate and potassium nitrate were purchased from Sigma-Aldrich. Aluminum wire (>99.9%) was obtained from Beijing Jiaming Non-ferrous Metals Industry Co., Ltd. (Beijing, China). Agar powder (CP) was purchased from Beijing Anboxing BLO-Tech. Comp. Ltd. (Beijing, China). All chemicals were of analytical grade and used without further purification. Deionized water generated by a Milli-Q system (Millipore, USA) with a resistivity higher than 18.2 MΩ was used in all experiments.

2.2 Preparation and characterization of silver films

Silver products were synthesized in a designed electrochemical reactor (shown in Fig. 1), which included two cells connected by a salt bridge and an electric wire. A zinc rod, placed in the potassium nitrate solution and serving as the anode, and an aluminum wafer, immersed in the silver nitrate solution and acting as the cathode, were connected by the wire. A voltage-stabilized (15 V) power supply was linked to the middle of the wire. The current density was regulated by the resistances. The electrons flowed across the nitrate silver solution through the cathode, forming silver particles on its surface. The aluminum wafer cathode had a diameter of 1.5 cm and a thickness of 1 mm. The backside of the wafer was covered by agar gel. All electrodes were washed with ethanol and pure water to clean their surfaces before immersion in the solution.

The electrochemical reaction was conducted in the designed reactor at room temperature (25 °C). The

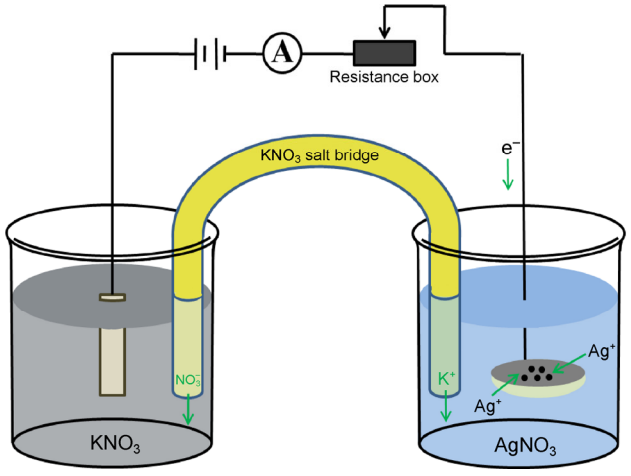

Figure 1 Schematic of the designed electrochemical reactor. Two vessels are connected by a salt bridge and an electronic wire. The silver ions are reduced by the electrons coming from the external power supply, forming silver particles on the surface of the cathode wafer.

electrochemical deposition was performed at various applied current densities, and the cathode coated with the silver product was gently removed from the solution for further characterization. The untreated samples were first characterized by scanning electron microscopy (SEM), then contact angles measurements were performed, and finally their antibacterial activity was evaluated.

To measure the sterilization rate of the samples, silver products were incubated in an *E. coli* strain (MG1655) solution. The strain was cultured in Luria-Bertani (LB) medium at 37 ˚C overnight, and then diluted into fresh LB medium with the designed volume ratio (2,000:1) in 6-well plates; all wells contained different samples, while one was left without sample as negative control. After culturing for 4 h, 350 μL of LB medium from each well was transferred into 96-well plates and measured for optical density (OD600) using a multilabel counter. The ratio of the OD600 of the sample to that of the control was quantitatively associated with the efficiency of the sterilization. Meanwhile, 150 μL of the strains cultured overnight in LB medium was laid in dishes with agar gel; then, the silver samples were placed in the dishes, while one dish was left without sample, as negative control. After culturing at 37 ˚C for 12 h, the photos of the bacterial colony in the dishes qualitatively showed the sample sterilization efficiency.

The morphology of the silver products was characterized by field-emission SEM (JSM-7001F) equipped with an energy-dispersive X-ray spectroscopy (EDS) analyzer. The phase and composition of the silver products were determined by X-ray diffraction (XRD; PANalyticalB.V., Netherlands), using CuKα radiation, and the data were collected over a 2θ range of 5°–90° at a scanning step of 0.1°. The contact angles of the samples were estimated using a contact angle measurement system (OCA-20, Dataphysics, Germany). The concentration of colibacillus was determined by a multilabel counter (Wallac Victor3 1420, PerkinElmer Life Sciences).

3 Results and discussion

The formation of silver particles on the surface of the cathode was monitored by sampling at different reaction times and analyzing the samples by SEM (Fig. 2). The electrodeposition was conducted at the current density of 500 μA/cm^2 in a 3 mM silver nitrate solution. In the initial stages of the reaction, spherical patterns were formed on the surface of the cathode, as shown in Fig. 2(a). As the reaction proceeded, the spherical patterns expanded, forming silver dendrites and polyhedrons on the surface of the cathode (Fig. 2(b)). More dendrites were progressively formed, leading to the formation of a silver film on the surface of the cathode (Figs. 2(c) and 2(d)). Both the XRD pattern

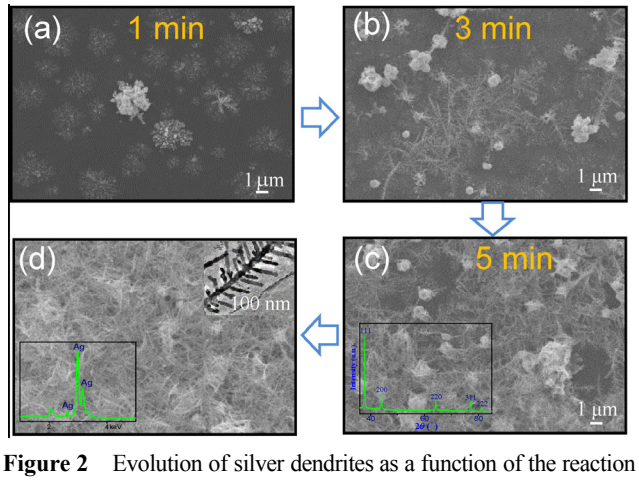

Figure 2 Evolution of silver dendrites as a function of the reaction time. Initially, silver nucleates on the surface of the cathode (a); as the reaction progresses, the nuclei grow up, forming dendritic structures (b) and (c), which completely cover the cathode after 10 min of reaction time (d).

(bottom-left inset of Fig. 2(c)) and EDS spectrum (bottom-left inset of Fig. 2(d)) revealed that the dendritic products consisted of silver. The top-right inset of Fig. 2(d) shows a magnification image of the silver particles forming the silver film on the cathode surface. The silver particles exhibited a dendritic structure with a thick trunk and many side branches. These results show that the formation of silver dendrites starts with the surface nucleation, then followed by the growth of silver dendritic structures, which are often produced during electrochemical depositions, especially in fine powdery deposition systems [37, 38]. Their formation was ascribed to the instability of the crystal growth front in a diffusion limited field, which was extensively investigated by many researchers, such as Sekerka and Mullins [39]. It was proposed that the formation of dendritic structures is controlled by the chemical gradient on the growth front of the crystals [40, 41].

To examine the surface properties of the silver film, we measured the contact angle of a water drop placed on it. The contact angle is the angle between a liquid/vapor interface and a solid surface when a water droplet rests on the surface of the solid. This angle is determined by the properties of both the solid and liquid, interaction and repulsion forces between liquid and solid, and interface properties of the three phases (gas, liquid, and solid). The contact angle of a water droplet placed on silver films formed at different reaction times, shown in Fig. 3, changed with the reaction time, suggesting its dependence on the morphology of the silver film. Both a loose coating, obtained after the initial reaction stages, and a dense coating, formed after 10 min of reaction, led to low contact angles, whereas the loose dendritic silver films formed after intermediate reaction times exhibited high contact angles (Fig. 3). Generally, the surface morphology plays an important role in the wetting behavior. The following contact angle model qualitatively illustrates how the factors determine the contact angle of a rough surface composed of solid and air [42].

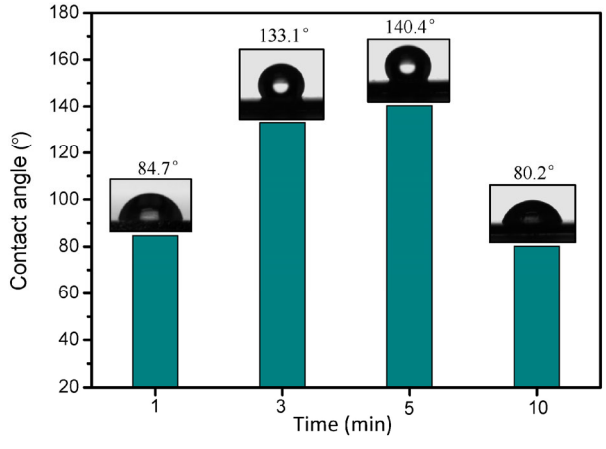

Figure 3 Contact angles of silver films prepared at different reaction times.

$$\cos\theta_c = f_s\cos\theta - f_a \quad f_s + f_a = 1$$
$$\cos\theta_c = f_s\cos\theta - (1 - f_s) = f_s(\cos\theta + 1) - 1 \qquad (1)$$

Here, θ_c is the contact angle of the rough film, θ is the contact angle of the flat surface of a solid, and f_s and f_a are the liquid-solid and liquid-air contact area fractions, respectively, with respect to the nominal contact area. Equation (1) clearly indicates that θ_c increases with the decrease of f_s, namely, θ_c increases with the fraction of air trapped on the film surface during the measurements. The contact angle (θ) is 110° for a smooth silver surface [43]. Hence, we can estimate that the f_s value of the sample synthesized after 5 min is ~0.35, which means that 65% (f_a = 0.65) of air is trapped in the silver dendritic film as a result of the loose dendritic coating.

Gu et al. reported, for their dendritic silver film, a contact angle of only 7.0° ± 1°, which increased to 154.5° ± 1.0° after modifying the surface of the film with n-dodecanethiol, as the modification produced a superhydrophobic surface [39]. However, without recurring to chemical modification, metallic micro and nanostructures with dual scale roughness may also confer hydrophobic properties to the surface [44]. Owing to the formation of dendritic silver particles, the contact angles of the silver films reached 140.4° after 5 min of deposition, as shown in Fig. 3. These results indicate that the hydrophobic activity is not only dependent on the density of the film, but also on the morphology of the silver particles. A short reaction time leads to the formation of a thin silver layer, as shown in Fig. 2(a). Both the morphology and density of the thin layer do not favor the hydrophobic interaction. After 10 min of reaction, when the dendritic silver particles expanded, only a small quantity of air was trapped in the silver film, and the hydrophobic

interaction was not favored. At the optimal deposition time of 5 min, the loosely dendritic silver films demonstrated a high hydrophobicity as a result of the high content of air in the film as well as the formation of dendritic structures.

To examine the antibiotic activity, silver films prepared at different reaction times were tested for inhibition zone and OD600 measurements, as shown in Fig. 4. Here, the antibacterial rates (r) were calculated by the following equation

$$r = (OD_c - OD_s)/OD_c$$

where OD_c and OD_s are the OD600 values of the control sample (without silver film) and test samples (with silver film), respectively. The silver products formed at the early stages of the reaction exhibit high antibacterial activities, while the products formed after 10 min showed a poor antibacterial activity, as shown in Fig. 4. The inhibition zones agree well with the OD600 measurements. Notably, size, shape, and quantity are three major factors influencing the antibiotic activity of the particles. Among these three factors, the size effect is remarkable. A smaller size leads to a higher antibiotic activity. There are at least two reasons to account for the size effect. First, particles with small sizes, especially nanometer sizes, can easily penetrate inside the bacteria by disrupting their membranes. Second, a small size is associated with a high surface free energy, which leads to a quick production of silver ions and ROS [20]. Therefore, small silver particles exhibit a more effective sterilization than larger particles,

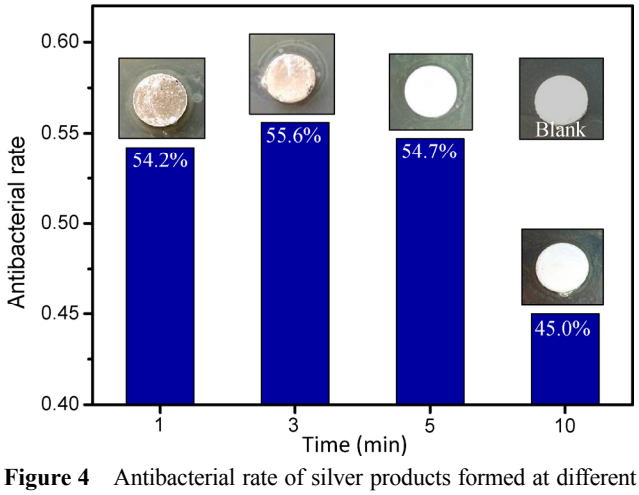

Figure 4 Antibacterial rate of silver products formed at different reaction times and corresponding images of the inhibition zones.

as it has been described by the Ostwald-Freundlich model [44]. As a result, the silver films synthesized at short reaction times have a high antibiotic activity due to the small size of their particles. Conversely, in the later stages of the reaction, the particles become too large, leading to a decrease of the antibiotic activity (Fig. 4).

Previous studies have shown that the morphology of the silver film was largely dependent on the applied current density [45, 46]. Hence, we compared the antibacterial rate and contact angle of silver films generated at different current densities (Fig. 5). By increasing the current density, both the antibacterial rate and contact angle increased. It has been reported that high current densities favor the nucleation process, resulting in a massive nucleation on the cathode surface and the formation of a rough surface. Therefore, as the increase of current density leads to an increase of hydrophobicity, the silver film synthesized at the current density of 750 μA/cm^2 exhibited superhydrophobicity with a contact angle of 150.9°. At the same time, the improvement of the nucleation process by the high current density prevented the excessive growth of the particles, leading to the formation of small particles and a high antibacterial activity (Fig. 5). By further increasing the current density to 1,000 μA/cm^2, many hydrogen bubbles gas were produced, which prevented the formation of a uniform silver film.

The morphology of the silver film is also dependent on the concentration of the silver salt [46]. At low concentration (1 mM), the limited nucleation and restricted growth of the silver particles led to the formation of a loose film with poor hydrophobic properties. Concurrently, the small silver particles on the surface of the cathode exhibited a strong antibacterial activity, as shown in Fig. 6. By increasing the salt concentration to 3 mM, dendritic structures were largely formed, generating a porous film on the cathode surface (Fig. 6), which resulted in a remarkable increase of the contact angles and a slight decrease of the antibacterial activity as a result of the larger size of the silver particles. The contact angles of the silver films are mainly determined by two aspects. One is the porosity of the film, or the content of air in the film, which has been discussed in the previous section. Another factor is the morphology of the silver particles.

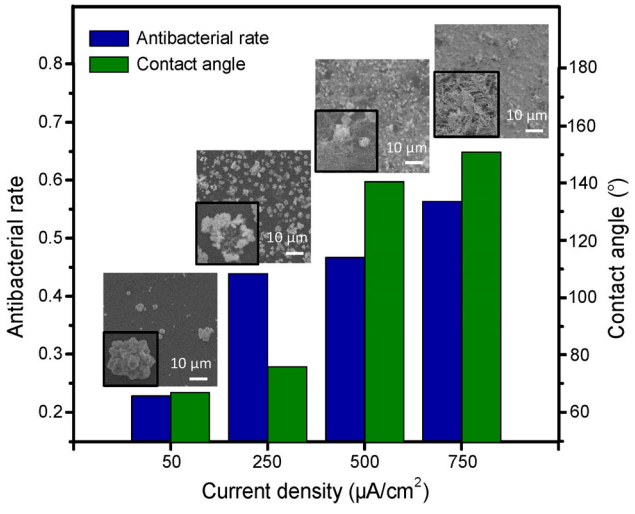

Figure 5 Antibacterial rate and contact angles of silver films synthesized at different current densities after 5 min of deposition.

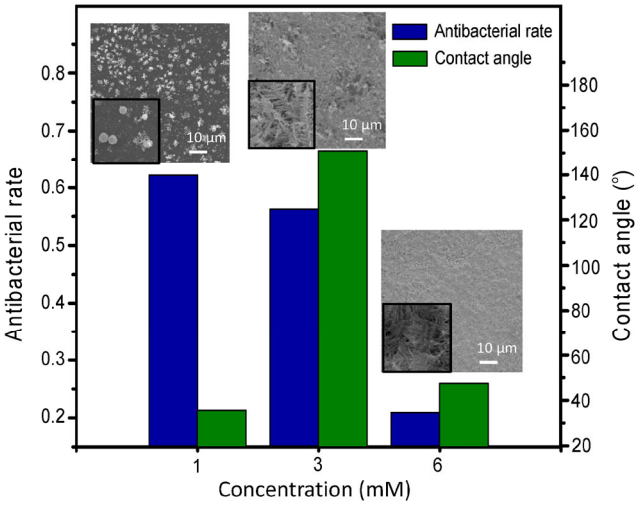

Figure 6 Antibacterial rate and contact angle of silver films fabricated at different concentrations of silver salt.

The dendritic particles of the silver film create a rough surface, which leads to the enhancement of the hydrophobic properties. Xue Y. et al. [47] fabricated a superhydrophobic surface by growing cobalt dendrites on the surface of a modified gold electrode. The cobalt dendrites grew vertically with respect to the electrode, forming a rough surface. However, for prolonged reaction times, the cobalt dendrites developed nicely, forming a dense film on the electrode, which led to a decrease of the contact angle as a result of the reduction of the air content in the film. Therefore, both the morphology and porosity of the silver film heavily affect the superhydrophobicity. Further increasing the salt concentration to 6 mM, a dense film composed of large silver dendrites was generated on the surface of the cathode, which led to the decrease of both the antibacterial rates and contact angles, as shown in Fig. 6.

The hydrophobic and antibacterial properties of the silver film derive from different types of structure. The size of the silver particles influences the antibacterial property, while the morphology and porosity of the silver film determines the hydrophobic activity. To obtain small-sized silver particles, the nucleation should be enhanced, while the growth of the particles should be restrained. A high current density leads to a high nucleation rate, which results in the formation of massive nuclei on the metal substrate. At low concentrations of silver salt and short reaction times, these nuclei retain a small size, which leads to a high antibacterial activity. On the other hand, the growth of the silver nuclei to form dendritic structures favor the hydrophobicity of the film, as the dendritic particles produce a porous film on the cathode surface, which is necessary for the hydrophobic character. Furthermore, the formation of dendritic structures increases the roughness of the film surface, leading to an enhancement of the hydrophobicity. However, the overgrowth of silver dendrites forming a dense film on the cathode leads to a decrease of the contact angle. Therefore, to obtain a highly hydrophobic silver film, the growth of the silver nuclei should be controlled, forming dendritic structures to create a porous film on the surface of the cathode. As a result, a massive nucleation and moderate deposition time favor both the antibacterial and hydrophobic properties. After clarifying the relationship between preparation, structure, and properties of the materials, a smart procedure was here designed to produce a multifunctional material, exploiting a compromise between different material structures obtained by controlling the nucleation and growth processes.

4 Conclusions

Multifunctional silver films were fabricated by the electrochemical method, obtaining a maximal contact angle of 150.9° and an optimal antibacterial rate of 54.7% for *E. coli*. By regulating the reaction time, the

silver concentration, and current density, silver films with diverse morphologies were generated and tested for antibacterial activity and hydrophobicity. The former was mainly dependent on the size of the silver particles, while the latter was determined by the morphology and density of the silver films. Small-sized silver particles, which were obtained by promoting the nucleation and limiting the growth, led to a high antibacterial activity. Superhydrophobicity was achieved with a rough silver film composed of dendritic particles, which were formed by controlling the growth of the silver particles. Therefore, after clarifying the relationship between material preparation, structure, and properties, a multifunctional silver film was prepared by controlling the nucleation and growth of the silver particles, showing that a compromise between different material structures is a smart way to prepare multifunctional materials.

Acknowledgements

This study was supported by the Hundreds Talent Program from the Chinese Academy of Sciences and the project from the State Key Laboratory of Multiphase Complex Systems (No. MPCS-2014-D-05). The financial support from National Natural Science Foundation of China (Nos. U1462130 and 21406232) is warmly appreciated.

References

[1] Chitwood, D. H.; Naylor, D. T.; Thammapichai, P.; Weeger, A. C. S.; Headland, L. R.; Sinha, N. R. Conflict between intrinsic leaf asymmetry and phyllotaxis in the resupinate leaves of alstroemeria psittacina. *Front. Plant Sci*. **2012**, *3*, 182.

[2] Beerling, D. J.; Osborne, C. P.; Chaloner, W. G. Evolution of leaf-form in land plants linked to atmospheric CO_2 decline in the Late Palaeozoic Era. *Nature* **2001**, *410*, 352–354.

[3] Jiang, Z. X.; Geng, L.; Huang, Y. D.; Guan, S. A.; Dong, W.; Ma, Z. Y. The model of rough wetting for hydrophobic steel meshes that mimic *Asparagus setaceus* leaf. *J. Colloid Interface Sci.* **2011**, *354*, 866–872.

[4] Burton, Z.; Bhushan, B. Surface characterization and adhesion and friction properties of hydrophobic leaf surfaces. *Ultramicroscopy* **2006**, *106*, 709–719.

[5] Tang, S. H.; Chen, M.; Zheng, N. F. Multifunctional ultrasmall Pd nanosheets for enhanced near-infrared photothermal therapy and chemotherapy of cancer. *Nano Res*. **2015**, *8*, 165–174.

[6] Park, S. H.; Cho, E. H.; Sohn, J.; Theilmann, P.; Chu, K. M.; Lee, S.; Sohn, Y.; Kim, D.; Kim, B. Design of multi-functional dual hole patterned carbon nanotube composites with superhydrophobicity and durability. *Nano Res*. **2013**, *6*, 389–398.

[7] Knight, R. J. B. The introduction of copper sheathing into the Royal Navy, 1779–1786. *The Mariner's Mirror* **1973**, *59*, 299–309.

[8] Harris, J. R. Copper and shipping in the eighteenth century. *Economic History Rev.* **1966**, *19*, 550–568.

[9] Teklu, B. M.; Adriaanse, P. I.; Ter Horst, M. M. S.; Deneer, J. W.; Van den Brink, P. J. Surface water risk assessment of pesticides in Ethiopia. *Sci. Total Environ*. **2015**, *508*, 566–574.

[10] Parrón, T.; Requena, M.; Hernández, A. F.; Alarcón, R. Environmental exposure to pesticides and cancer risk in multiple human organ systems. *Toxicol. Let*. **2014**, *230*, 157–165.

[11] Hu, X. N.; Zhao, Y. Y.; Hu, Z. J.; Saran, A.; Hou, S.; Wen, T.; Liu, W. Q.; Ji, Y. L.; Jiang, X. Y.; Wu, X. C. Gold nanorods core/AgPt alloy nanodots shell: A novel potent antibacterial nanostructure. *Nano Res*. **2013**, *6*, 822–835.

[12] Fasciani, C.; Silvero, M. J.; Anghel, M. A.; Arguello, G. A.; Becerra, M. C.; Scaiano, J. C. Aspartame-stabilized gold–silver bimetallic biocompatible nanostructures with plasmonic photothermal properties, antibacterial activity, and long-term stability. *J. Am. Chem. Soc*. **2014**, *136*, 17394–17397.

[13] Yuan, X.; Setyawati, M. I.; Leong, D. T.; Xie, J. P. Ultrasmall Ag^+-rich nanoclusters as highly efficient nanoreservoirs for bacterial killing. *Nano Res*. **2014**, *7*, 301–307.

[14] Choi, O.; Deng, K. K.; Kim, N. J.; Ross, L. Jr.; Surampalli, R. Y.; Hu, Z. Q. The inhibitory effects of silver nanoparticles, silver ions, and silver chloride colloids on microbial growth. *Water Res*. **2008**, *42*, 3066–3074.

[15] Choi, O.; Hu, Z. Q. Size dependent and reactive oxygen species related nanosilver toxicity to nitrifying bacteria. *Environ. Sci. Technol*. **2008**, *42*, 4583–4588.

[16] Reyes-Vidal, Y.; Suarez-Rojas, R.; Ruiz, C.; Torres, J.; Ţălu, Ş.; Méndez, A.; Trejo, G. Electrodeposition, characterization, and antibacterial activity of zinc/silver particle composite coatings. *Appl. Surf. Sci*. **2015**, *342*, 34–41.

[17] Morones, J. R.; Elechiguerra, J. L.; Camacho, A.; Holt, K.; Kouri, J. B.; Ramírez, J. T.; Yacaman, M. J. The bactericidal

effect of silver nanoparticles. *Nanotechnology* **2005**, *16*, 2346–2353.

[18] AshaRani, P. V.; Low Kah Mun, G.; Hande, M. P.; Valiyaveettil, S. Cytotoxicity and genotoxicity of silver nanoparticles in human cells. *ACS Nano* **2009**, *3*, 279–290.

[19] Sondi, I.; Salopek-Sondi, B. Silver nanoparticles as antimicrobial agent: A case study on *E. coli* as a model for Gram-negative bacteria. *J. Colloid Interface Sci*. **2004**, *275*, 177–182.

[20] Batchelor-McAuley, C.; Tschulik, K.; Neumann, C. C. M.; Laborda, E.; Compton, R. G. Why are silver nanoparticles more toxic than bulk silver? Towards understanding the dissolution and toxicity of silver nanoparticles. *Int. J. Electrochem. Sci*. **2014**, *9*, 1132–1138.

[21] Chen, S. F.; Li, J. P.; Qian, K.; Xu, W. P.; Lu, Y.; Huang, W. X.; Yu, S. H. Large scale photochemical synthesis of M@TiO_2 nanocomposites (M = Ag, Pd, Au, Pt) and their optical properties, CO oxidation performance, and antibacterial effect. *Nano Res*. **2010**, *3*, 244–255.

[22] Sivera, M.; Kvitek, L.; Soukupova, J.; Panacek, A.; Prucek, R.; Vecerova, R.; Zboril, R. Silver nanoparticles modified by gelatin with extraordinary pH stability and long-term antibacterial activity. *PLoS One* **2014**, *9*, e103675.

[23] Bing, W.; Chen, Z. W.; Sun, H. J.; Shi, P.; Gao, N.; Ren, J. S.; Qu, X. G. Visible-light-driven enhanced antibacterial and biofilm elimination activity of graphitic carbon nitride by embedded Ag nanoparticles. *Nano Res*. **2015**, *8*, 1648–1658.

[24] Zhang, W.; Yao, Y.; Sullivan, N.; Chen, Y. S. Modeling the primary size effects of citrate-coated silver nanoparticles on their ion release kinetics. *Environ. Sci. Technol*. **2011**, *45*, 4422–4428.

[25] Shrivastava, S.; Bera, T.; Roy, A.; Singh, G.; Ramachandrarao, P.; Dash, D. Characterization of enhanced antibacterial effects of novel silver nanoparticles. *Nanotechnology* **2007**, *18*, 225103.

[26] Sadeghi, B.; Garmaroudi, F. S.; Hashemi, M.; Nezhad, H. R.; Nasrollahi, A.; Ardalan, S.; Ardalan, S. Comparison of the anti-bacterial activity on the nanosilver shapes: Nanoparticles, nanorods and nanoplates. *Adv. Powder Technol*. **2012**, *23*, 22–26.

[27] Bansal, V.; Li, V.; O'Mullane, A. P.; Bhargava, S. K. Shape dependent electrocatalytic behaviour of silver nanoparticles. *CrystEngComm* **2010**, *12*, 4280–4286.

[28] Wang, H.; Yang, J. T.; Li, X. L.; Zhang, H. Z.; Li, J. H; Guo, L. Facet-dependent photocatalytic properties of AgBr nanocrystals. *Small* **2012**, *8*, 2802–2806.

[29] Pal, S.; Tak, Y. K.; Song, J. M. Does the antibacterial activity of silver nanoparticles depend on the shape of the nanoparticle? A study of the gram-negative bacterium *Escherichia coli*. *Appl. Environ. Microbiol*. **2007**, *73*, 1712–1720.

[30] Fan, W. H.; Wang, X. L.; Cui, M. M; Zhang, D. F.; Zhang, Y.; Yu, T.; Guo, L. Differential oxidative stress of octahedral and cubic Cu_2O micro/nanocrystals to *Daphnia magna*. *Environ. Sci. Technol*. **2012**, *46*, 10255–10262.

[31] Xu, X. H.; Zhang, Z. Z.; Yang, J. Fabrication of biomimetic superhydrophobic surface on engineering materials by a simple electroless galvanic deposition method. *Langmuir* **2010**, *26*, 3654–3658.

[32] Su, B.; Wang, S. T.; Song, Y. L.; Jiang, L. A miniature droplet reactor built on nanoparticle-derived superhydrophobic pedestals. *Nano Res*. **2011**, *4*, 266–273.

[33] Kang, S. M.; You, I.; Cho, W. K.; Shon, H. K.; Lee, T. G.; Choi, I. S.; Karp, J. M.; Lee, H. One-step modification of superhydrophobic surfaces by a mussel-inspired polymer coating. *Angew. Chem., Int. Ed*. **2010**, *49*, 9401–9404.

[34] Lu, Y.; Sathasivam, S.; Song, J. L.; Crick, C. R.; Carmalt, C. J.; Parkin, I. P. Robust self-cleaning surfaces that function when exposed to either air or oil. *Science* **2015**, *347*, 1132–1135.

[35] Song, Y.; Nair, R. P.; Zou, M.; Wang, Y. Q. Superhydrophobic surfaces produced by applying a self-assembled monolayer to silicon micro/nano-textured surfaces. *Nano Res*. **2009**, *2*, 143–150.

[36] Wu, L. K.; Hu, J. M.; Zhang, J. Q.; Cao, C. N. Superhydrophobic surface constructed on electrodeposited sol-gel silica film. *Electrochem. Commun*. **2013**, *26*, 85–88.

[37] Mendoza-Reséndez, R.; Gómez-Treviño, A.; Barriga-Castro, E. D.; Núñez, N. O.; Luna, C. Synthesis of antibacterial silver-based nanodisks and dendritic structures mediated by royal jelly. *RSC Adv*. **2014**, *4*, 1650–1658.

[38] Zhu, J.; Kim, K. S.; Liu, Z. X.; Feng, H.; Hou, S. F. Electroless deposition of silver nanoparticles on graphene oxide surface and its applications for the detection of hydrogen peroxide. *Electroanalysis* **2014**, *26*, 2513–2519.

[39] Sekerka, R. F. A stability function for explicit evaluation of the Mullins–Sekerka interface stability criterion. *J. Appl. Phys*. **1956**, *36*, 264–268.

[40] Zhao, Q.; Li, J.; Tang, S. Y.; Zhang, Y. Z.; Chen, L.; Choi, M. M. F.; Guo, Y.; Xiao, D. Magnetic-field-induced growth of silver dendrite-crystalline Liesegang rings. *CrystEngComm* **2014**, *16*, 6542–6546.

[41] Fang, J. X.; You, H. J.; Zhu, C.; Kong, P.; Shi, M.; Song, X.

P.; Ding, B. J. Thermodynamic and kinetic competition in silver dendrite growth. *Chem. Phys. Lett*. **2007**, *439*, 204–208.

[42] Cassie, A. B. D. Contact angles. *Discuss. Faraday Soc*. **1948**, *3*, 11–16.

[43] Gu, C. D.; Zhang, T. Y. Electrochemical synthesis of silver polyhedrons and dendritic films with superhydrophobic surfaces. *Langmuir* **2008**, *24*, 12010–12016.

[44] Ostwald, W. Z. Blocking of Ostwald ripening allowing long-term stabilization. *Phys. Chem*. **1901**, *37*, 385.

[45] Liu, W.; Yang, T.; Li, C. X.; Che, P.; Han, Y. S. Regulating silver morphology via electrochemical reaction. *CrystEngComm* **2015**, *17*, 6014–6022.

[46] Yang, T.; Han, Y. S.; Li, J. H. Manipulating silver dendritic structures via diffusion and reaction. *Chem. Eng. Sci*. **2015**, *138*, 457–464.

[47] Xue, Y. P.; Taleb, A.; Jegou, P. Electrodeposition of cobalt films with an oriented fir tree-like morphology with adjustable wetting properties using a self-assembled gold nanoparticle modified HOPG electrode. *J. Mater. Chem*. **2013**, *1*, 11580–11588.